

Supporting Information for

Manipulating the Ion-Transference Kinetics and Interface Stability for High-Performance Zinc Metal Anode

Xuesong Xie,^a Shuquan Liang,^a Jiawei Gao,^a Shan Guo,^a Jiabao Guo,^a Chao Wang,^b Guiyin Xu,^b
Xianwen Wu,^c Gen Chen,^a and Jiang Zhou,^{*a}

*a School of Materials Science and Engineering, Central South University, Changsha 410083,
Hunan, P.R. China. E-mail: zhou_jiang@csu.edu.cn*

*b Department of Nuclear Science and Engineering, Massachusetts Institute of Technology,
Cambridge, MA 02139, USA.*

c School of Chemistry and Chemical Engineering, Jishou University, Jishou 416000, P.R. China

Experimental Section

Synthesis: All the reagents are of analytical purity and used as received without further purification. Firstly, the high concentrated $Zn(OH)_4^{2-}$ the solution was prepared by the mixed with potassium hydroxide (KOH) and zinc nitrate ($Zn(NO_3)_2 \cdot 6H_2O$), where 11.55 g $Zn(NO_3)_2 \cdot 6H_2O$ and 8.97 g KOH was separately dissolved into 40 mL distilled water. And then, the KOH solution was added drop by drop to the $Zn(NO_3)_2$ solution with water bath at 308 K. As the addition of KOH solution, the transparent solution was transformed into white precipitation and after the centrifugation at 8600 r/min for 15 min, the solution of $Zn(OH)_4^{2-}$ was complete finished. The area of 10 cm² pristine Zn foil (0.1 mm thickness with a purity of 99.99 %) was immersed into the as-prepared solution with following reaction of $Zn(OH)_4^{2-} \rightarrow ZnO \downarrow + 2 H_2O + 2 OH^-$ at the temperature of 308 K. After immersed for 5 min with constant ultrasound treatment, the resulting as-prepared anode washed by distilled water several times to remove the unwanted ionic species (K^+ , NO_3^-). The comparison group of ZnO coating was prepared by mixing the 80 wt % nano-ZnO with the size range of 20 ~ 40 nm (99.9 %, Aladdin) and 20 wt % polyvinylidene fluoride (PVDF) with suitable NMP solution. And then the slurry directly coated on the zinc foil and dried on the 343 K oven for 10 h. The thickness is measured by the spiral micrometer.

Characterization: Powder X-ray diffraction (XRD) patterns were conducted by the Rigaku Mini Flex 600 diffractometer using Cu K_α -radiation ($\lambda = 1.5418$) with a scan speed of 2°/min. XPS measurements were carried out on an ESCALAB 250 Xi X-ray photoelectron spectrometer (Thermo Fisher). Morphology images were collected on a FESEM (FEI Nova NanoSEM 230, 10kV) field emission scanning electron microscope. Electron probe microanalysis was performed on a JXA-8230 instrument with wavelength-dispersive X-ray spectroscopy (WDS) characterization. The high/low-temperature performance was conducted by using a high/low-temperature test box (LAND GT2001B, China).

Electrochemical Measurement: The cathode electrodes were composed of MnO_2 , conductive carbon black and PVDF at a mass ratio of 7:2:1. The bare Zn and as-prepared Zn@ZnO-3D were punched into disks ($\Phi = 15$ mm) and served as the counter electrode. The cathode and anode electrodes were separated by glass fiber separators ($\Phi = 19$ mm, Whatman). 2 M $ZnSO_4$ + 0.1 M

MnSO₄ aqueous solution was used as the typically liquid electrolyte. The cells were assembled in the air atmosphere. Galvanostatic charge/discharge cycling measurements were carried out on a LAND multichannel battery test system (CT2001A, China). EIS and CV data of the batteries was recorded on the electrochemical workstation (CHI660E, China). Galvanostatic intermittent titration technique (GITT) was used to conduct the chemical diffusion of Zinc (D_{zn}) at different states *via* the Arbin instruments system at room temperature. Linear sweep voltammetry (LSV) was carried out at a scan rate of 5 mV s⁻¹ in 0.1 M H₂SO₄ solution after a purging of Ar (99.999%) in 8 h. The measurement is conducted in the three-electrode systems at room temperature that Zn plate (1.0 cm²), glass carbon and Ag/AgCl (3.5 M KCl) adopted as the working, counter and a reference electrode, respectively.

DFT calculations: The calculation was implemented in the Vienna ab-initio simulation package (VASP) *via* the first principle plane-wave pseudopotential formation and with the generalized gradient approximation of Perdew–Burke–Ernzerhof (PBE) form. For optimizing the crystal structure, cutoff energy of 400 eV and a Monkhorst–Pack k-mesh of 4 × 4 × 1 were employed. The energy convergence was set to less than 10⁻⁵ eV and the residual force on each atom was less than 0.03 eV/ Å. In this model, A 20 Å vacuum was added into the z-direction. The five-layer Zn(001) slab with dimensions of 7.9 Å × 7.9 Å × 22.8 Å was used, and the bottom of 2 layers was fixed.

The binding energy of Zn@ZnO-3D and bare Zn with extra Zn element is following as:

$$E_{Zn-Zn@ZnO-3D} = E_{Zn+Zn@ZnO-3D} - E_{Zn@ZnO-3D} - E_{Zn}$$

$$E_{Zn-Bare Zn} = E_{Zn+Bare Zn} - E_{Bare Zn} - E_{Zn}$$

where the $E_{Zn+Zn@ZnO-3D}$ and $E_{Zn+bare Zn}$ are presented the total energies of the metal intercalated bulk of Zn@ZnO-3D and bare Zn after the absorption of Zn. $E_{Zn@ZnO-3D}$, $E_{Bare Zn}$, and E_{Zn} are the total energies of the pristine Zn@ZnO-3D, pristine bare Zn and the isolated metal Zn atom, respectively.

Figures and Tables

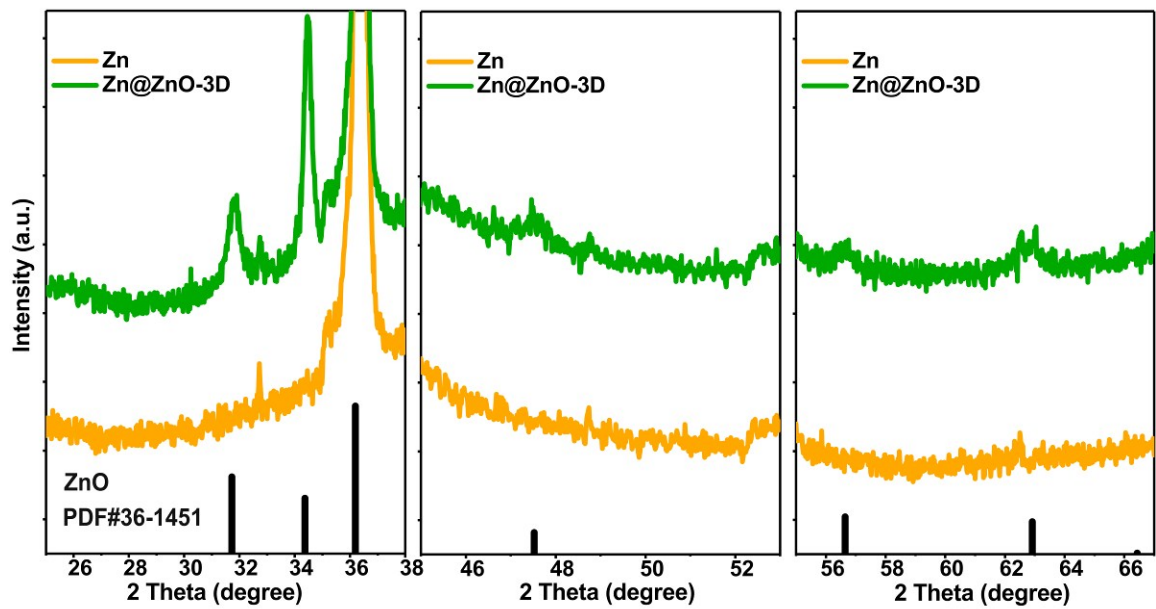


Fig. S1 The XRD patterns of Zn@ZnO-3D and bare Zn.

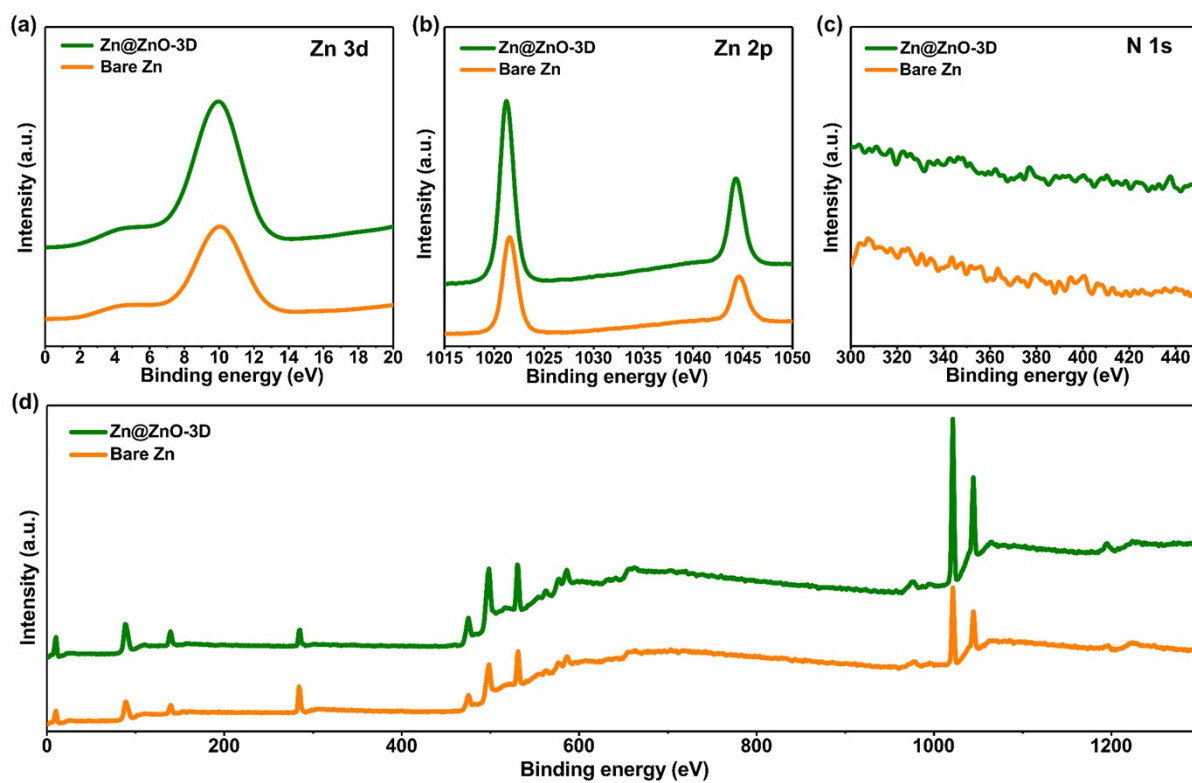


Fig. S2 The Zn 3d (a), Zn 2p (b), N 1s (c), and full XPS peaks (d) for Zn@ZnO-3D and bare Zn, respectively.

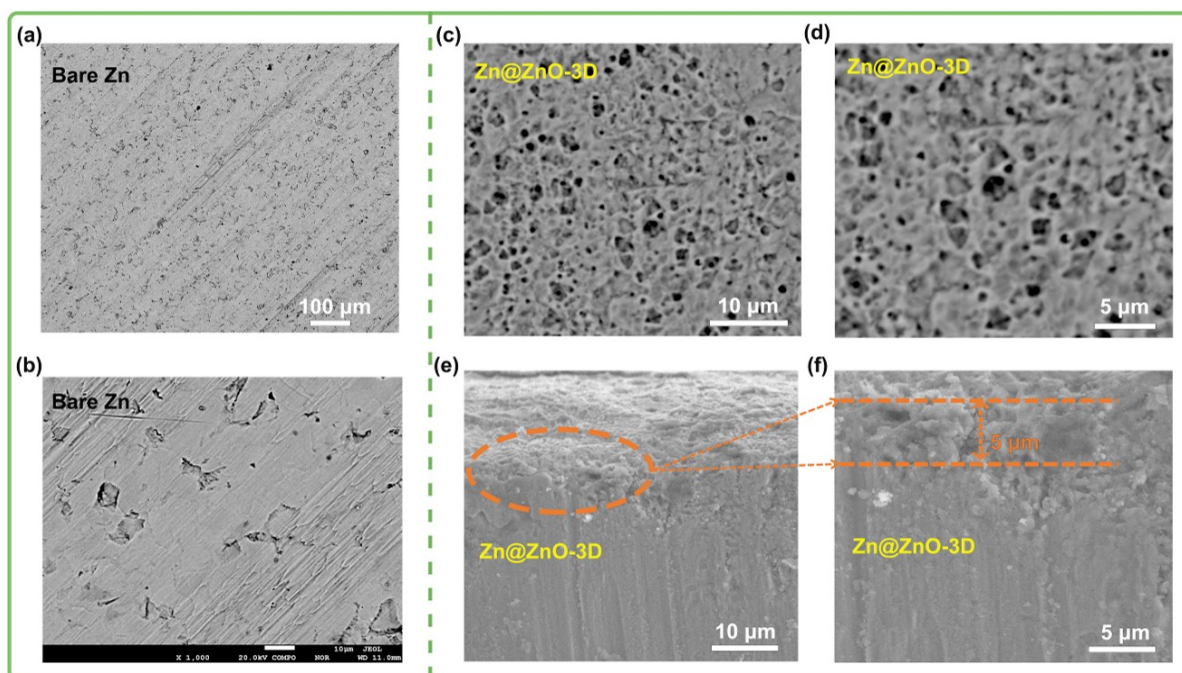


Fig. S3 Backscatter electron images (BSE) of bare Zn anode at a low (a) and high (b) magnification, and the Zn@ZnO-3D anode at low (c) and (d) resolution. Cross-section morphology (SEM) of Zn@ZnO-3D at low (e) and high (f) resolution.

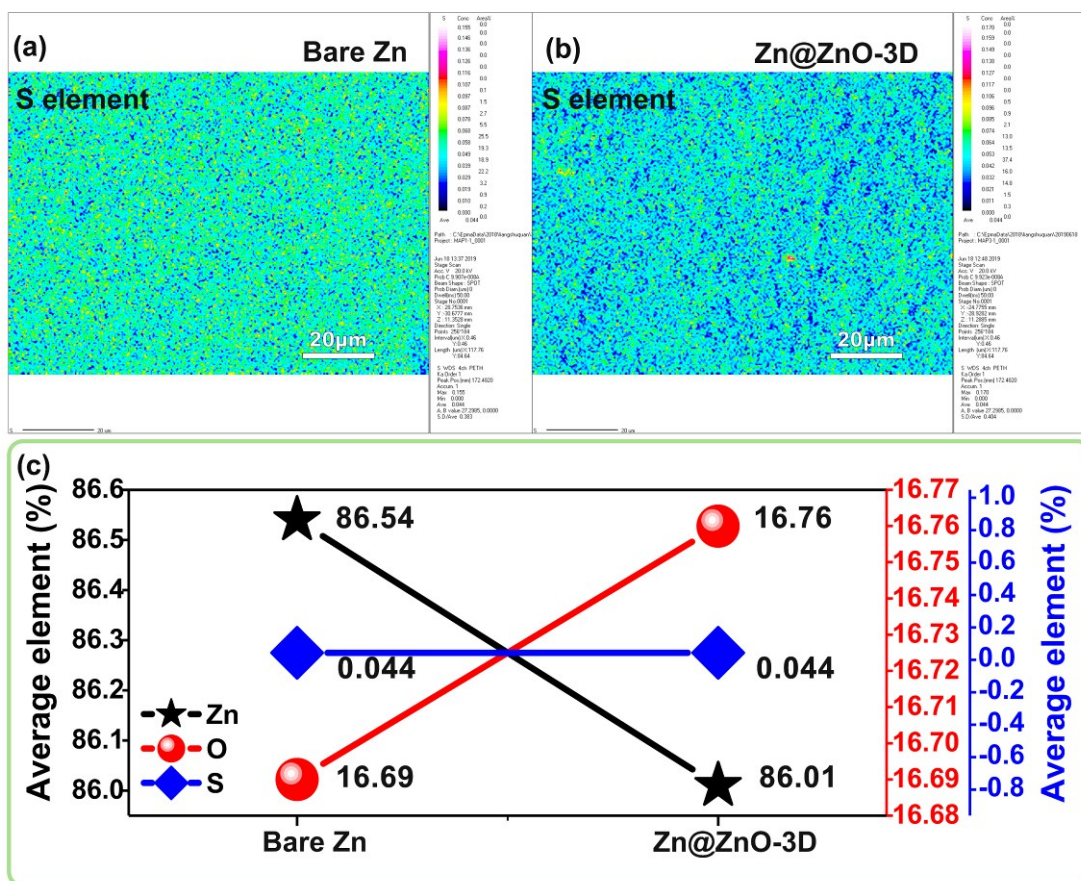


Fig. S4 The EMPA/WDS element distribution of S element for bare Zn (a) and Zn@ZnO-3D (b). c)

Precise data comparison ratio of Zn, O, S elements for Zn@ZnO-3D and bare Zn.

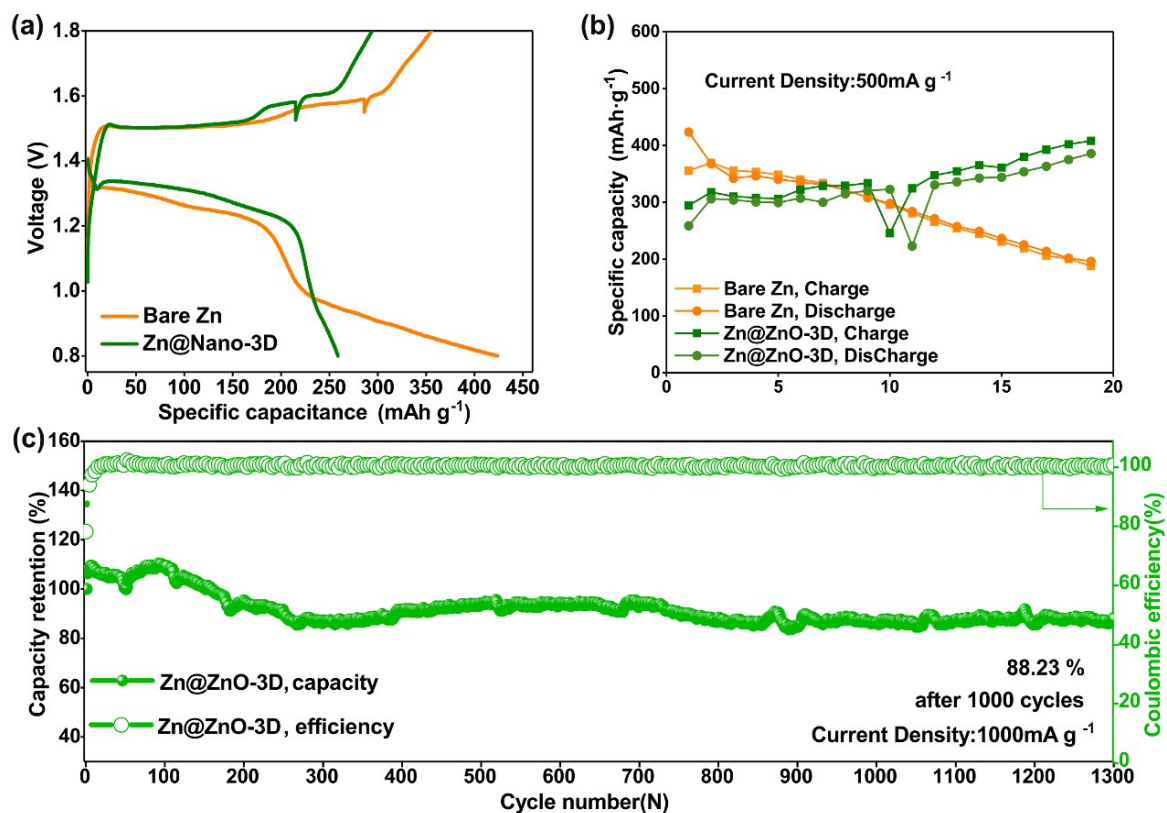


Fig. S5 a) First charge-discharge curves and cycling performance of bare Zn and Zn@ZnO-3D at a current density of 50 mA g⁻¹ (b), and capacity retention of Zn@ZnO-3D/MnO₂ full cell at a current density of 1000 mA g⁻¹ (c).

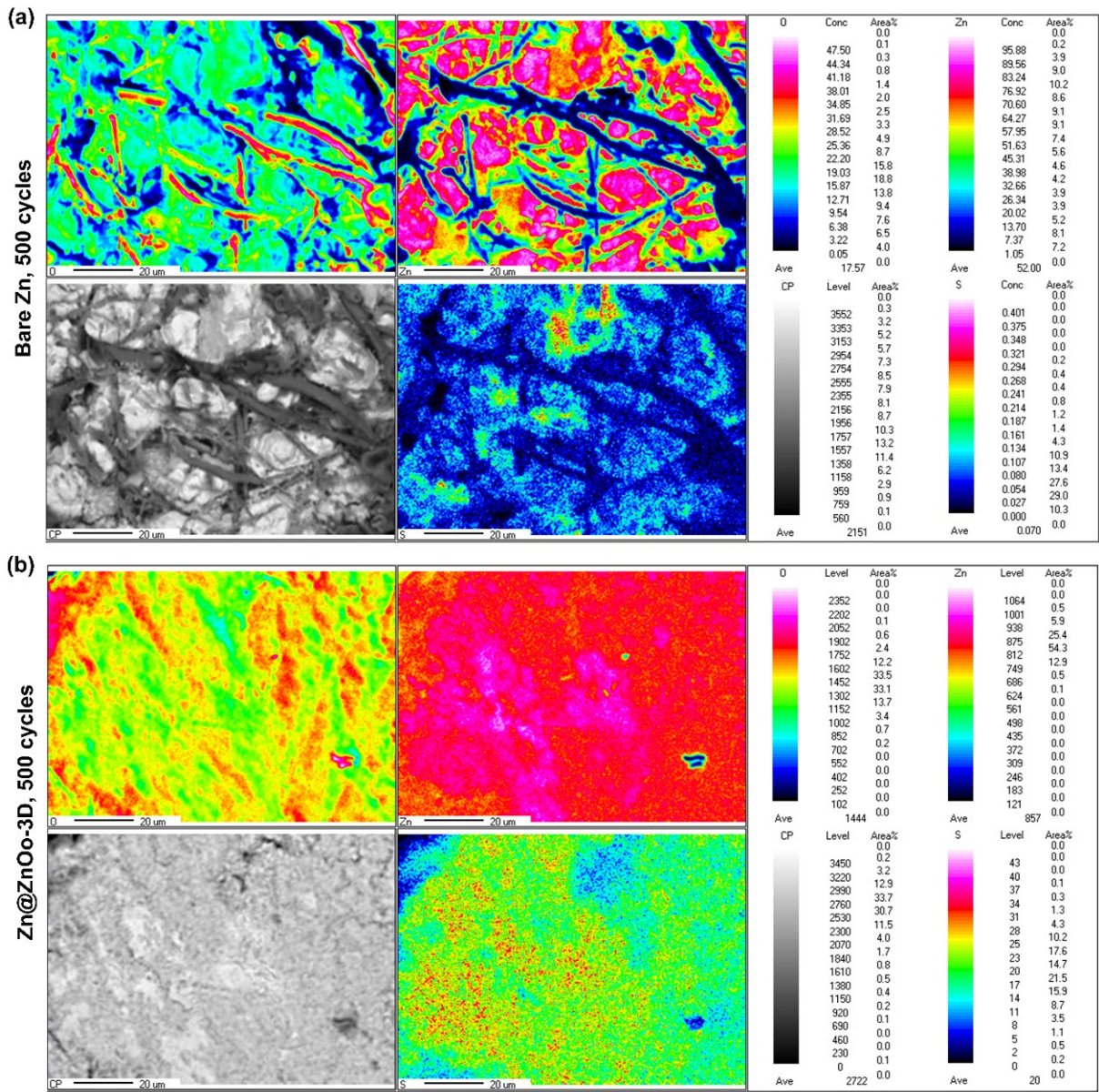


Fig. S6 Corresponding EPMA mapping (O, Zn, S) and WDS results of bare Zn (a) and Zn@ZnO-3D (b) after 500 cycles.

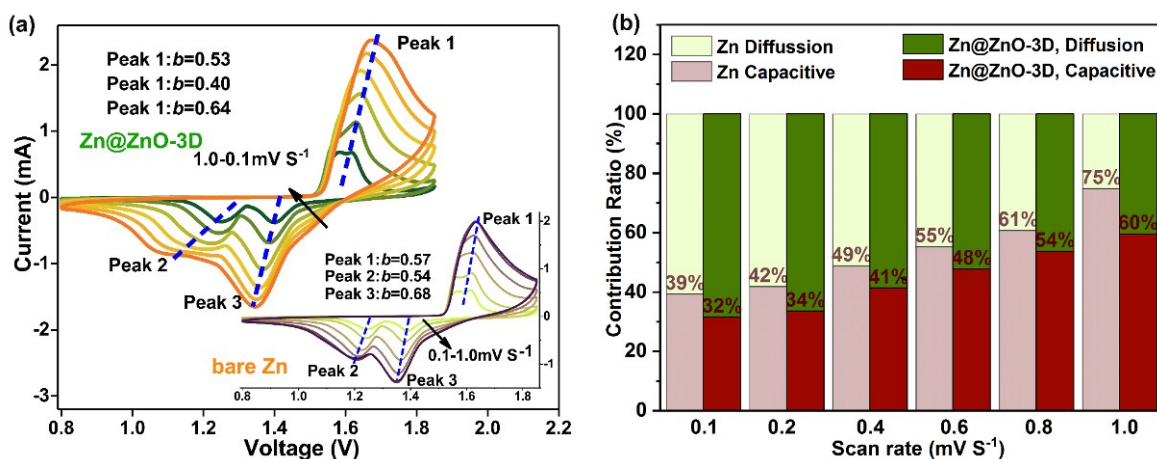


Fig. S7 (a) Cyclic voltammetry (CV) curves at different scan rates for MnO₂ cells cycled with Zn@ZnO-3D and bare Zn, respectively. (b) Corresponding percent of capacitive and diffusion contribution.

For kinetics comparison, it is because the change of current peak will be related to the scan rates, thus this trend could reveal the kinetics of zinc insertion/extraction at the solid electrolyte interfaces. The b value calculated by the power-law, $i = av^b$, where the b value of 0.5 is of battery-type diffusion behavior whereas $b = 1$ means a capacitive-controlled process. Further information is provided by the equation $i = k_1v + k_2v^{1/2}$, in which diffusion contribution ($k_2v^{1/2}$) and capacity contribution (k_1v) could be quantified under the different scan rates.

In this respect, the kinetics and quantitative analysis of Zn²⁺ storage capability were performed by CV curves at scan rates from 0.1 to 1.0 mV s⁻¹ as shown in Fig. S8a. As for the Zn@ZnO-3D, the b values (calculated by the power-law,¹ $i = av^b$) of three redox peaks (0.53, 0.40, and 0.64) all tightly close to 0.5, demonstrating a solid-state ion diffusion process. Further information is observed in Fig. S8b, Zn@ZnO-3D is superior to that of bare Zn for diffusion contribution ratio at each of scan rates, such as at 1.0 mV s⁻¹ scan rate the diffusion capacity of Zn@ZnO-3D (40 %) is 1.6 times than the bare Zn (25 %), strongly suggesting the faster kinetic endowed by artificial interfaces.

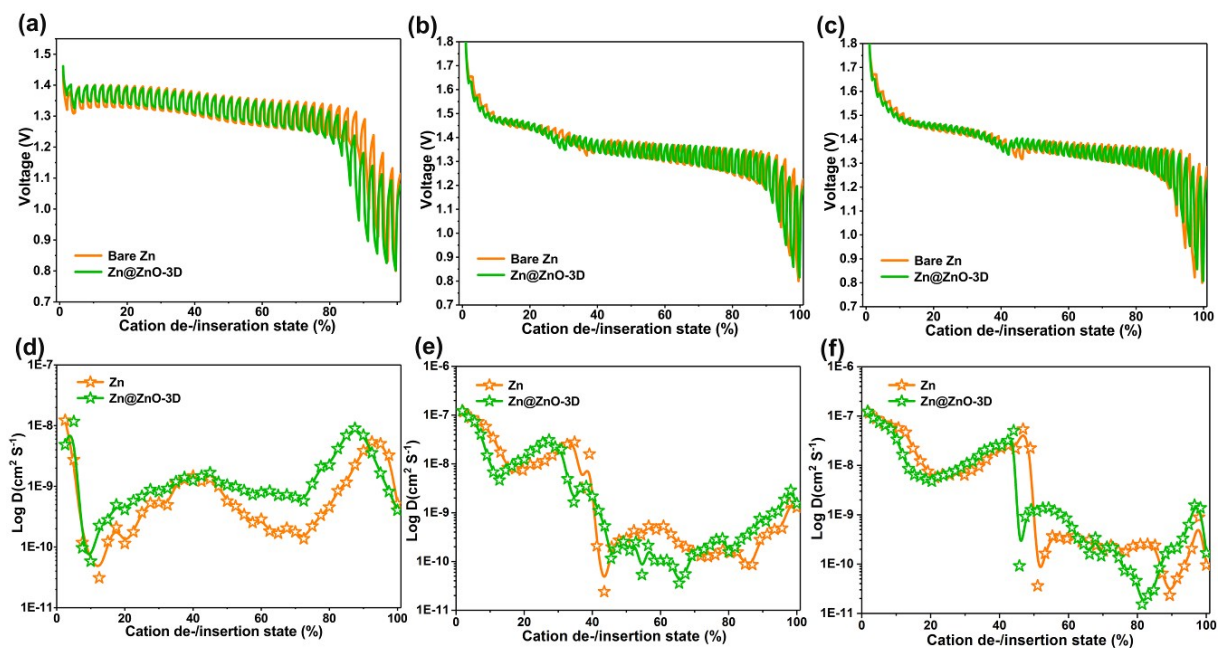


Fig. S8 GITT and diffusion coefficient contrast curve of full cells cycled with Zn@ZnO-3D and bare Zn electrode at first (a, d), second (b, e), and third (c, f) discharge process, respectively.

The galvanostatic intermittent titration technique (GITT) test of Zn@ZnO-3D anode also exhibits a higher Zn²⁺ diffusion coefficient D_{Zn} value. The detail calculation process is listed in Fig. S9. These results suggest that Zn@ZnO-3D could improve the kinetically ion diffusion process for the full cells.

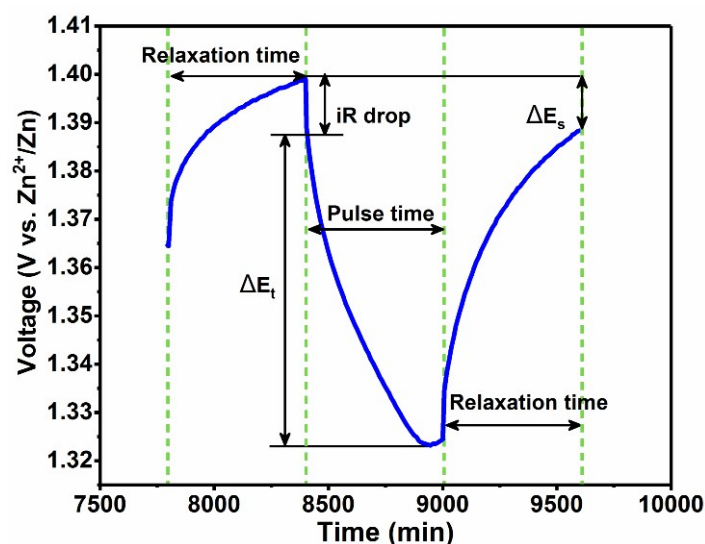


Fig. S9 E vs. t curves of the MnO_2 electrode cycled with Zn@ZnO-3D anode for a one GITT during the first discharge process. The diffusion coefficient was conducted by using Galvanostatic Intermittent Titration Technique (GITT) and calculated based on Eq. as follows:²

$$D = \frac{4L^2}{\pi t} \left(\frac{\Delta E_s}{\Delta E_t} \right)^2$$

Where t is the duration of the current pulse (s), ΔE_s is the steady-state potential change (V) by the current pulse. ΔE_t is the potential change (V) of the constant current pulse excluded the iR drop. L is ion diffusion length (cm); for compact electrode, it is equal to the thickness of the electrode. The galvanostatic intermittent titration technique (GITT) test for that Zn@ZnO-3D effect was carried out to estimate the chemical diffusion coefficients for that effect of Zn@ZnO-3D anode, where the cell was charged/discharged at a constant current 50 mA g^{-1} for an interval of 10 min and then suspended for 10 min at open-circuit state.

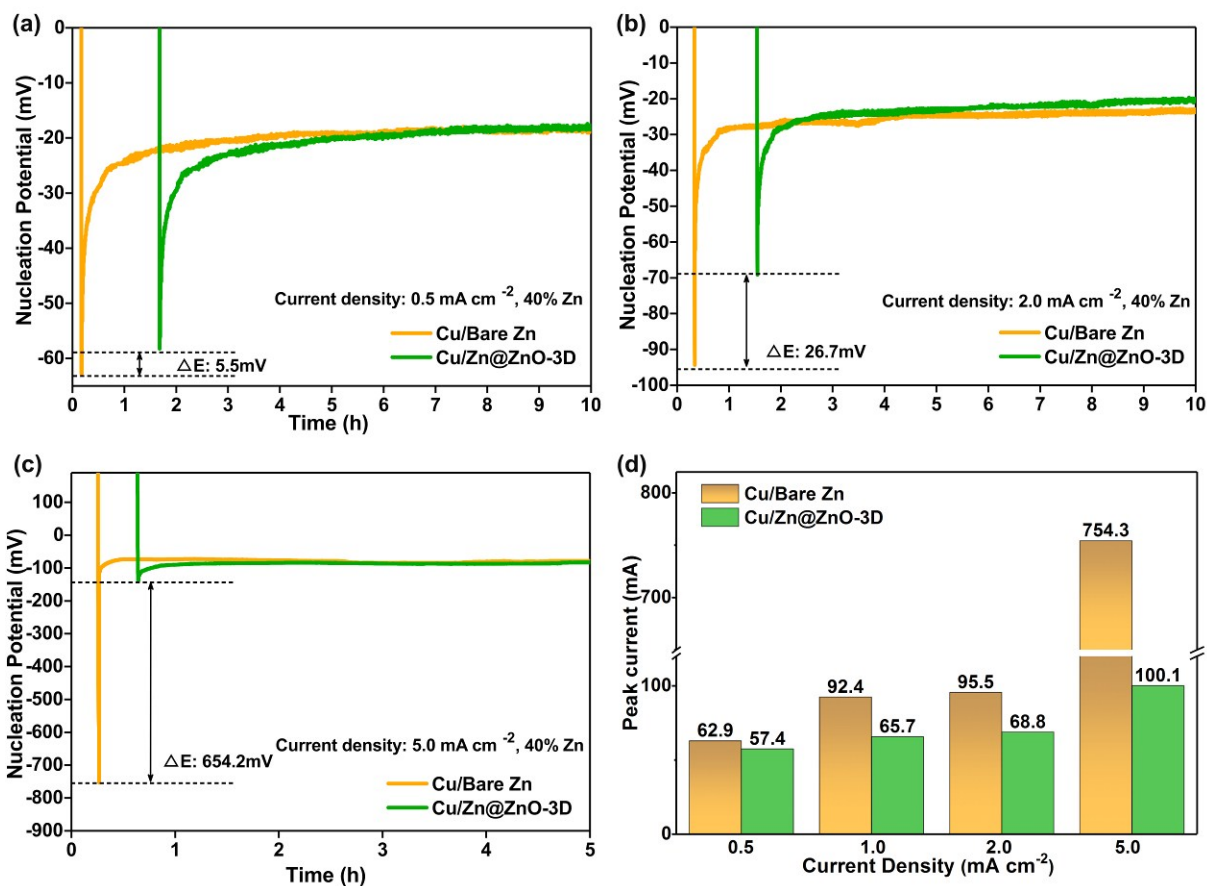


Fig. S10 Galvanostatic nucleation overpotential based on Cu matrix for Zn@ZnO-3D and bare Zn at a different density of (a) 0.5 mA cm⁻², (b) 2.0 mA cm⁻², (c) 5.0 mA cm⁻² and (d) histogram comparisons of corresponding peak current.

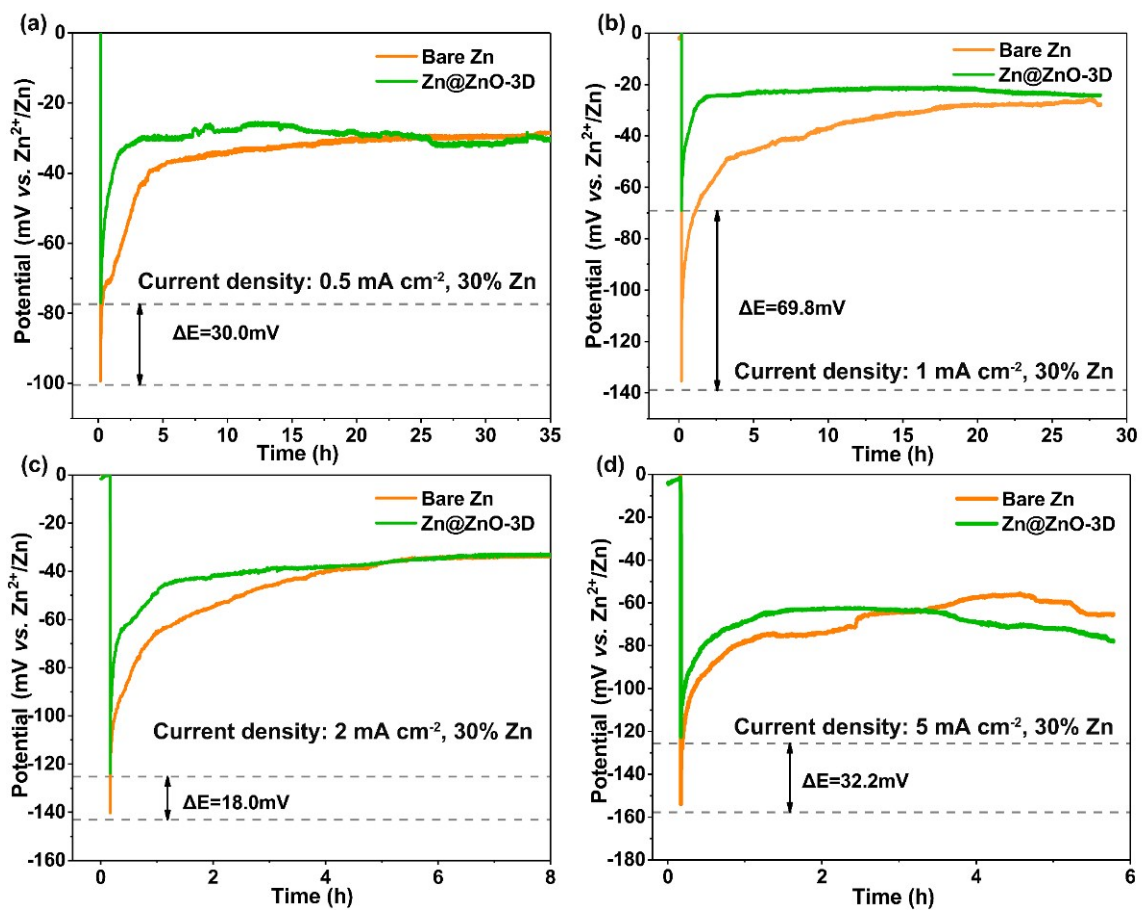


Fig. S11 Nucleation overpotential based on Zn matrix for Zn@ZnO-3D and bare Zn at different densities of (a) 0.5 mA cm^{-2} , (b) 1.0 mA cm^{-2} , (c) 2.0 mA cm^{-2} and (d) 5.0 mA cm^{-2} .

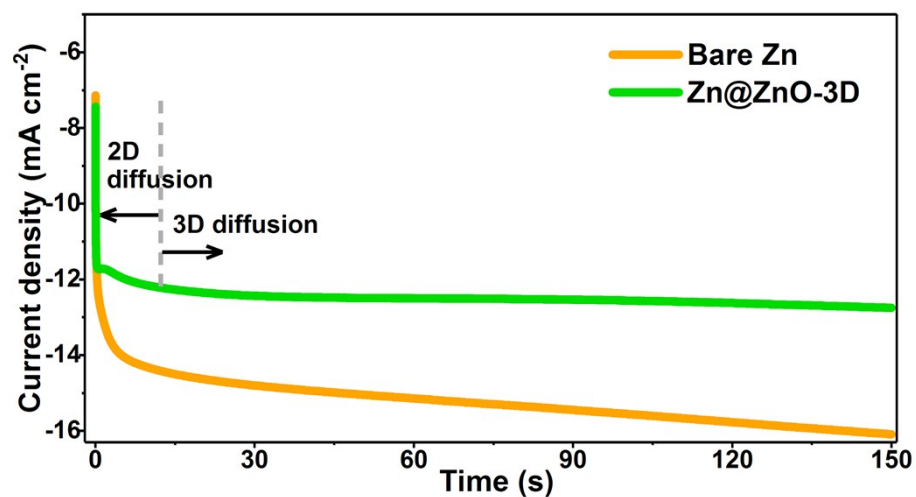


Fig. S12 Chronoamperometry (CA) curves of Zn@ZnO-3D and bare Zn at a constant potential of -150 mV. The nucleation mechanism and deposition process are performed by chronoamperometry (CA) measurement because of the sensitive relationship of the current curve toward the electrode surface area during plating.

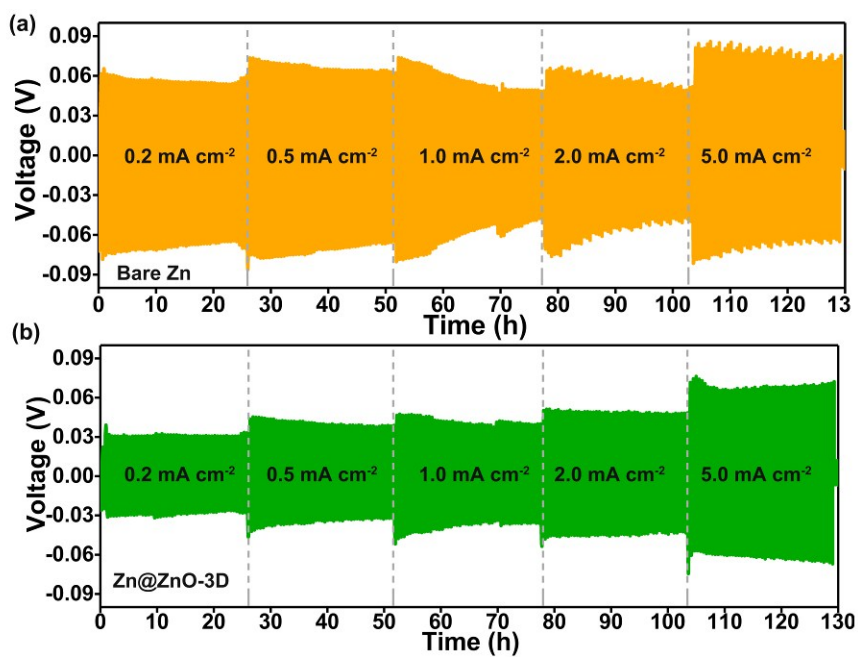


Fig. S13 Galvanostatic cycling performance of symmetric cells of (a) bare Zn and (b) Zn@ZnO-3D at various current densities from 0.2 mA cm⁻² to 5.0 mA cm⁻² for extracting the overpotential at each current and plotting the over-potential *versus* current curves to calculate the exchange current density of Zn²⁺ plating/stripping process.

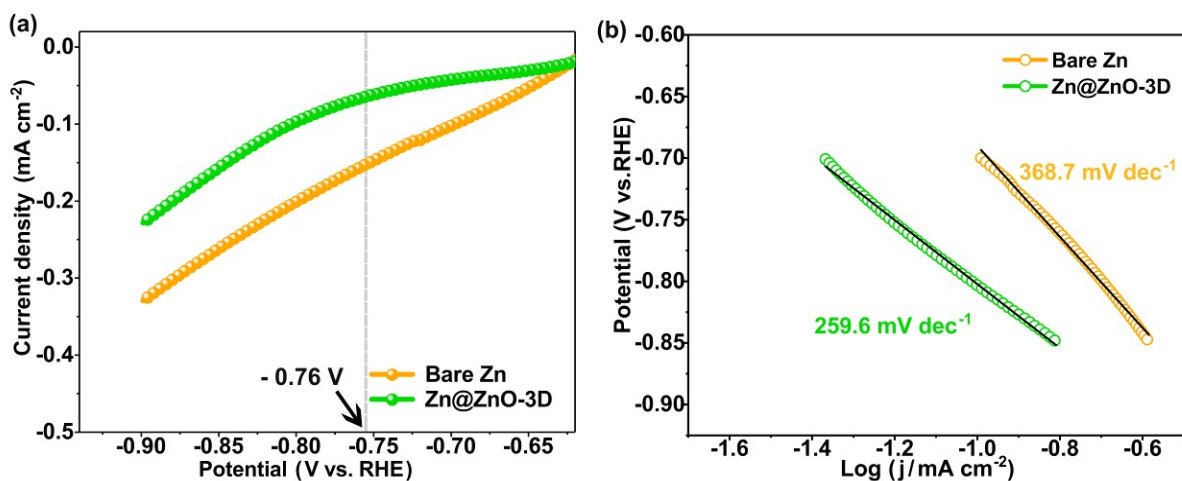


Fig. S14 (a) Linear sweep voltammetry (LSV) of Zn@ZnO-3D and bare Zn at a scan rate of 5 mV s⁻¹ in 0.1 M H₂SO₄ solution with a purging of Ar (99.999%) in 8 h and (b) corresponding Tafel curves. The measurement is conducted in the three-electrode systems at room temperature where Zn plate (1.0 cm²), glass carbon and Ag/AgCl (3.5 M KCl) adopted as the working, counter and a reference electrode, respectively.

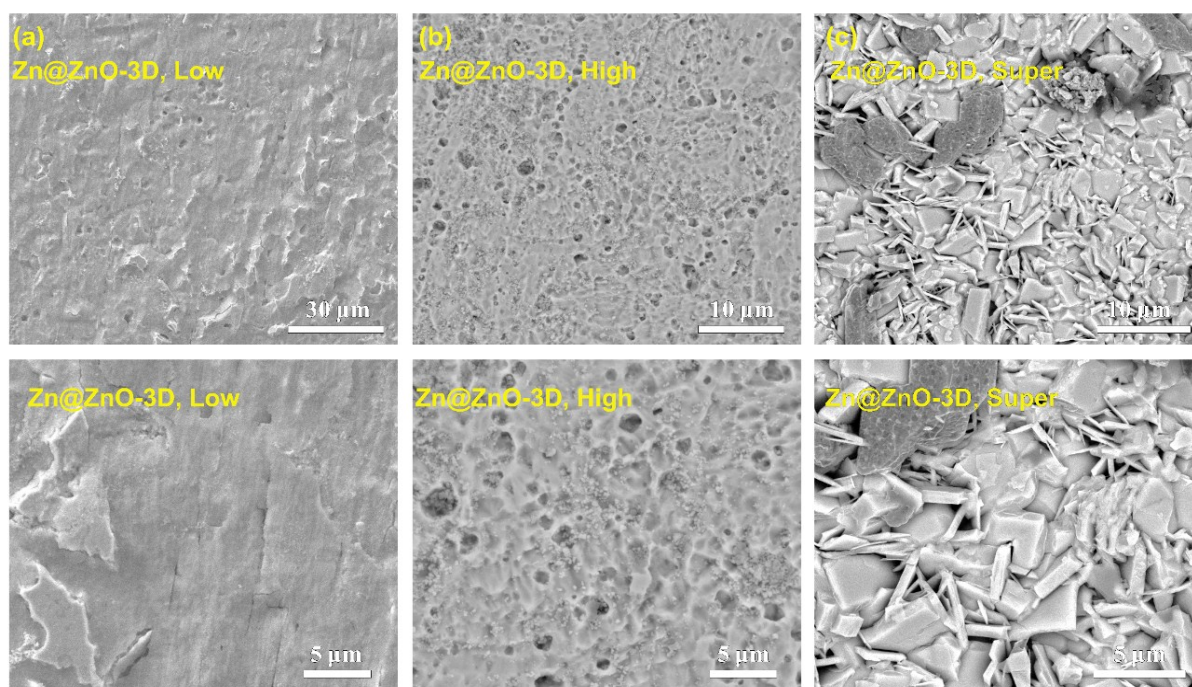


Fig. S15 SEM images of Zn@ZnO-3D anodes with different preparation environment of low (a), high (b), and super (c) concentration reactant.

As shown in Fig. S15, the Zn@ZnO-3D (Low, 0.2 Mol L⁻¹ Zn(NO₃)₂ 6H₂O + 1.0 Mol L⁻¹ KOH) exhibits a scatter of porous structure at that surface, which may be attributed to the sluggish reaction kinetics in that solution. A normal 3D architecture of anode is observed in that Zn@ZnO-3D (Middle, Fig. 1h-i) and Zn@ZnO-3D (High). While the Zn@ZnO-3D (Supper) exhibits a random block of zinc hydroxide or sulfate, which confirmed by the XRD characterization as shown in Fig. S16a.

As consistent with morphology, the electrochemical performance of Zn@ZnO-3D/MnO₂ full cells was measured, respectively. As shown in Fig. S16b, the Zn@ZnO-3D anode (High) exhibits the superior capacity retention than that of Zn@ZnO-3D (Low) at a current density of 0.5 A g⁻¹, which is in good consistency with the low resistance of EIS results (Fig. 3c) and the 3D architecture anode of SEM results that mentioned. The Zn@ZnO-3D (Super) manifests the worst one with a specific capacity of 98.9 mAh g⁻¹ after 200 cycles. It may be attributed to the random block of zinc hydroxide or nitrate at the anode surface hindering the Zn²⁺ transference.

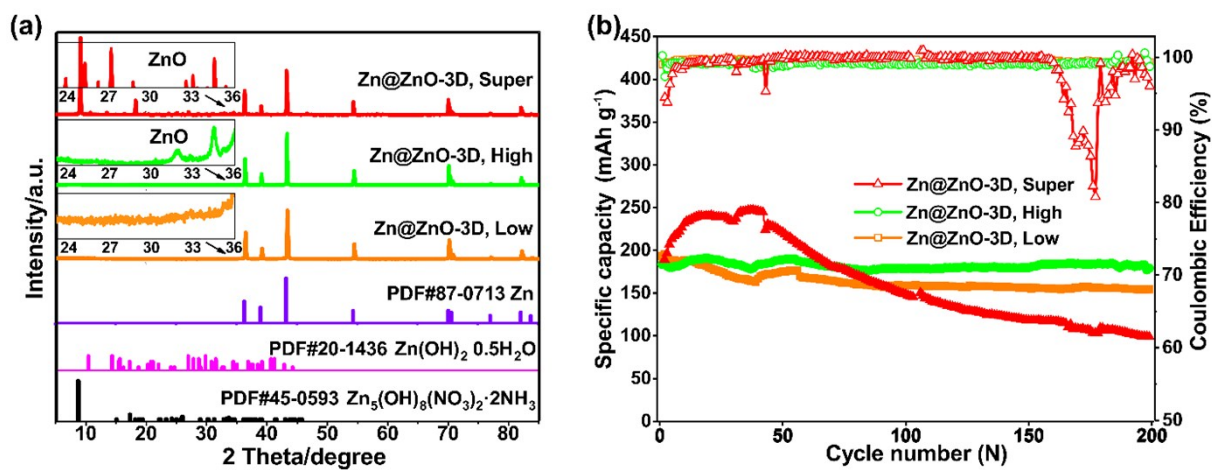


Fig. S16 (a) XRD patterns of Zn@ZnO-3D and corresponding cycling performance of Zn/MnO₂ full cells based on Zn@ZnO-3D anodes prepared by the different preparation conditions of low, high, and super concentration reactant.

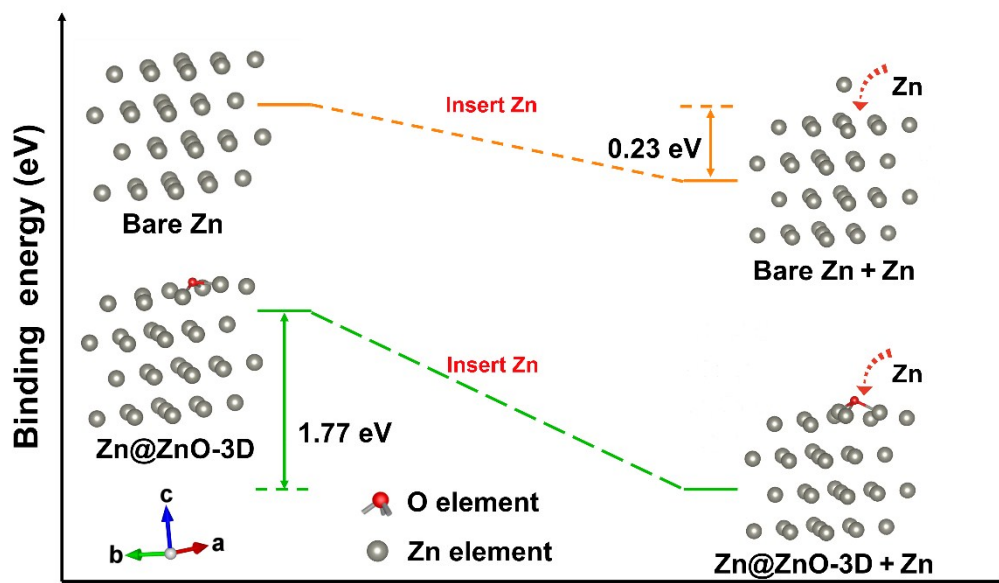


Fig. S17 The calculation of Zn insertion energy barriers for Zn@ZnO-3D and bare Zn.

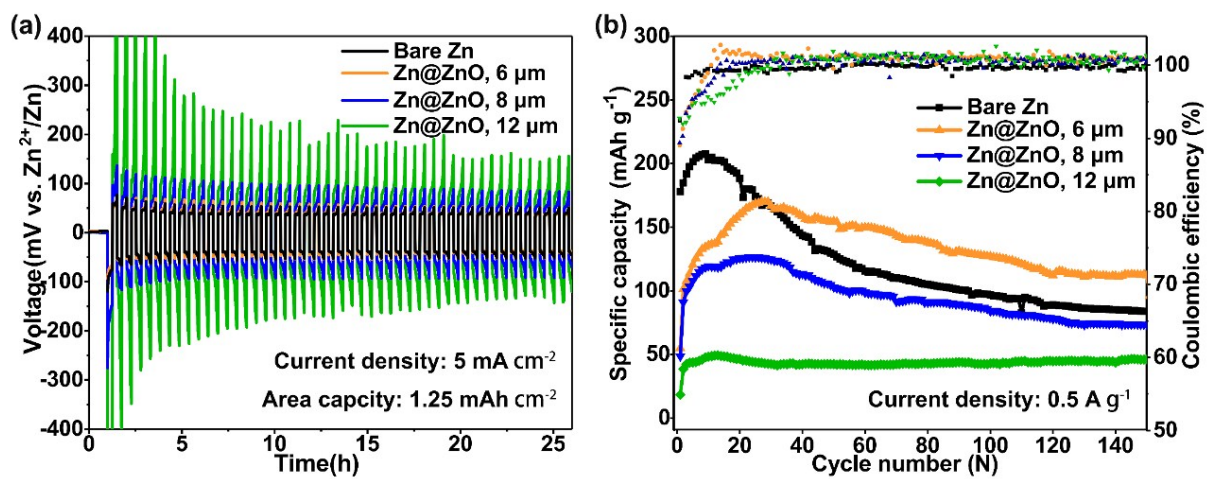


Fig. S18 (a) Galvanostatic cycling results of symmetrical ZnO-coated anodes (Zn@ZnO with different thickness of 6 μm, 8 μm, and 12 μm, respectively) and bare Zn at a current density of 5 mA cm⁻² with area capacity of 1.25 mAh cm⁻². (b) The corresponding cycling performance of full cells at a current density of 0.5 A g⁻¹.

Table S1 Exchange current density of hydrogen evaluation (I_H^2) for Zn@ZnO-3D and bare Zn when overpotential is reached 0 V, respectively.

Sampel	a/mV	$b/\text{mV dec}^{-1}$	$I_H^2/\text{mA cm}^{-2}$
Bare Zn	1059	368.7	1.34×10^{-3}
Zn@ZnO-3D	1062	259.6	8.11×10^{-5}

The calculation of exchange current density was followed by using the Tafel equation: ³

$$\eta = a + b \log(i) \quad (\text{S1})$$

The Tafel parameters are the intercept, a , which is actually $\log(i_o)$, and the slope, b . The linear scan voltammogram generated during the HER measurement (Fig. S14) is replotted in the form of the overpotential, η , vs. $\log(i)$. The resulting graph is known as a Tafel plot, and Tafel parameters can be determined by fitting the linear portion of the plot. The intercept is then used to determine i_o .

Table S2 Nyquist results of Zn@ZnO-3D symmetric cells fitting using the equivalent circuit with different preparation environment and the bare Zn.

Symmetric Cells	Zn(NO ₃) ₂ 6H ₂ O (Mol L ⁻¹)	KOH (Mol L ⁻¹)	R_{ct} (Ω)	R_s (Ω)
Bare Zn	/	/	1240	2.847
Zn@ZnO-3D, Super	2.0	3.0	761.5	4.1
Zn@ZnO-3D, High	1.0	2.0	635.4	4.331
Zn@ZnO-3D, Middle	0.5	2.0	292.7	0.98
Zn@ZnO-3D, Low	0.2	1.0	296.9	0.96

Table S3 The fitting resistance results of symmetric cells for Zn@ZnO-3D (using the Middle ones) and bare Zn by the equivalent circuit (same as the Fig. 3c fitting model) at different temperatures.

Symmetric Cells	Resistance (Ω)	0 °C (Ω)	10 °C (Ω)	20 °C (Ω)	25 °C (Ω)	40 °C (Ω)	60 °C (Ω)
Bare Zn/Zn	R_{ct}	18433	6648	2206	953.6	216.4	41.08
	R_s	5.912	7.714	7.222	4.458	7.077	8.282
Zn@ZnO-3D	R_{ct}	5536	2161	853.3	546.9	175.9	57.96
	R_s	9.135	6.27	7.828	5.578	6.731	7.7

Table S4 Comparison of typical parameters and cycling performance for this work with recently reported Zn-based symmetric cell.

Electrode	Electrolyte	Current density (mA cm ⁻²)	Capacity (mA h cm ⁻²)	Voltage hysteresis (mV)	DOD (%)	Life (h)	Reference
Zn@ZnO-3D	2M ZnSO₄ + 0.1M MnSO₄	5	1.25	43	~1.3	500	This work
Zn/SS mesh	3M Zn(CF ₃ SO ₃) ₂	2	1	~50	/	300	4
CNT-Zn	2M ZnSO ₄	2	2	27	~0.7	200	5
CC-Zn	2M ZnSO ₄	2	2	34	~0.7	53	
CaCO ₃ coated Zn	3M ZnSO ₄ + 0.1M MnSO ₄	2	0.1	100	/	80	6
Zn@ZIF-8	2M ZnSO ₄	1	1	25	/	50	7
Zn powder	1M Zn(TFSI) ₂ + 20M LiTFSI	0.2	0.068	~150	/	~170	8
Zn plate @TiO ₂	3 M Zn(CF ₃ SO ₃) ₂ + 0.1M Mn(CF ₃ SO ₃) ₂	1	1	~57.2	/	150	9
Zn foil	water@ZnMOF-808 solid-electrolyte	0.1	0.01	~100	/	360	10
Zn plate	0.5 M Zn(CF ₃ SO ₃) ₂ in triethyl phosphate : H ₂ O (7:3)	1	1	~200	/	200	11
3D anode onto Cu skeleton	2M ZnSO ₄	0.5	0.5	40	/	350	12

Table S5 Comparison of typical parameters and cycling performance for this work with recently reported Zn-based full cell.

Cathode	Anode	Electrolyte	Capacity (mA h g ⁻¹)	Capacity retention (%)	Current density (mA g ⁻¹)	Reference
α -MnO ₂	Zn@ZnO- 3D	2 M ZnSO ₄ + 0.1 M MnSO ₄	258.8 at 50 mA g ⁻¹	93.99 % after 500 cycles (212 mAh g⁻¹) 88.23 % after 1300 cycles	500 1000	This work
β -MnO ₂	Zn plate	3 M Zn(CF ₃ SO ₃) ₂ + 0.1 M Mn(CF ₃ SO ₃) ₂	275 at 200 mA g ⁻¹	81.81 % after 150 cycles (225 mAh g ⁻¹)	200	13
α -MnO ₂	Zn foil	2 M ZnSO ₄ + 0.1M MnSO ₄	285 at 103 mA g ⁻¹	~270 mAh g ⁻¹ after 60 cycles	308	14
σ -MnO ₂	Zn plate	1 M ZnSO ₄ + 0.2 M MnSO ₄	345 at 200 mA g ⁻¹	84 % after 2000 cycles	5000	15
MnO ₂	Zn-deposited	PVA / ZnCl ₂ / MnSO ₄ gel electrolyte	~340 at 0.74 A g ⁻¹	83.7 % after 300 cycles	1100	16
MnO ₂ @P EDOT	Zn-deposited		366 at 0.74 A g ⁻¹	47.2 % after 300 cycles	1100	
MnO ₂ @P EDOT	Zn/CNT	PVA - 2 M ZnCl ₂ - 0.4 M MnSO ₄	~300 at 2 mA cm ⁻²	88.7 % after 1000 cycles (167 mAh g ⁻¹)	20 mA cm ⁻²	5
MnO ₂ @P EDOT	Zn/CC		~269 at 2 mA cm ⁻²	69.7 % after 1000 cycles (~110 mAh g ⁻¹)		
β -MnO ₂	Zn foil	1 M ZnSO ₄	270 at 100 mA g ⁻¹	75% after 200 cycles	200	17
α -MnO ₂	3D Zn	2M ZnSO ₄ + 0.5 MnSO ₄	364 at 100 mA g ⁻¹	~65 % after 300 cycles (173 mA h g ⁻¹)	400	12

References

1. V. Augustyn, J. Come, M. A. Lowe, J. W. Kim, P. L. Taberna, S. H. Tolbert, H. D. Abruna, P. Simon and B. Dunn, *Nat. Mater.*, 2013, **12**, 518-522.
2. G. Fang, C. Zhu, M. Chen, J. Zhou, B. Tang, X. Cao, X. Zheng, A. Pan and S. Liang, *Adv. Funct. Mater.*, 2019, **29**, 1808375.
3. I. J. Hsu, Y. C. Kimmel, X. Jiang, B. G. Willis and J. G. Chen, *Chem. Commun.*, 2012, **48**, 1063-1065.
4. J. Zhao, H. Ren, Q. Liang, D. Yuan, S. Xi, C. Wu, W. Manalastas, J. Ma, W. Fang, Y. Zheng, C.-F. Du, M. Srinivasan and Q. Yan, *Nano Energy*, 2019, **62**, 94-102.
5. Y. Zeng, X. Zhang, R. Qin, X. Liu, P. Fang, D. Zheng, Y. Tong and X. Lu, *Adv. Mater.*, 2019, **31**, e1903675.
6. L. Kang, M. Cui, F. Jiang, Y. Gao, H. Luo, J. Liu, W. Liang and C. Zhi, *Adv. Energy Mater.*, 2018, **8**, 1801090.
7. Z. Wang, J. Huang, Z. Guo, X. Dong, Y. Liu, Y. Wang and Y. Xia, *Joule*, 2019, **3**, 1289-1300.
8. F. Wang, O. Borodin, T. Gao, X. Fan, W. Sun, F. Han, A. Faraone, J. A. Dura, K. Xu and C. Wang, *Nat. Mater.*, 2018, **17**, 543-549.
9. K. Zhao, C. Wang, Y. Yu, M. Yan, Q. Wei, P. He, Y. Dong, Z. Zhang, X. Wang and L. Mai, *Adv. Mater. Interfaces*, 2018, **5**, 1800848.
10. Z. Wang, J. Hu, L. Han, Z. Wang, H. Wang, Q. Zhao, J. Liu and F. Pan, *Nano Energy*, 2019, **56**, 92-99.

11. A. Naveed, H. Yang, J. Yang, Y. Nuli and J. Wang, *Angew. Chem., Int. Ed.*, 2019, **58**, 2760-2764.
12. Z. Kang, C. Wu, L. Dong, W. Liu, J. Mou, J. Zhang, Z. Chang, B. Jiang, G. Wang, F. Kang and C. Xu, *ACS Sustainable Chem. Eng.*, 2019, **7**, 3364-3371.
13. N. Zhang, F. Cheng, J. Liu, L. Wang, X. Long, X. Liu, F. Li and J. Chen, *Nat Commun.*, 2017, **8**, 405.
14. H. Pan, Y. Shao, P. Yan, Y. Cheng, K. S. Han, Z. Nie, C. Wang, J. Yang, X. Li, P. Bhattacharya, K. T. Mueller and J. Liu, *Nat. Energy*, 2016, **1**, 16039.
15. T. Xiong, Z. G. Yu, H. Wu, Y. Du, Q. Xie, J. Chen, Y. W. Zhang, S. J. Pennycook, W. S. V. Lee and J. Xue, *Adv. Energy Mater.*, 2019, **9**, 1803815.
16. Y. Zeng, X. Zhang, Y. Meng, M. Yu, J. Yi, Y. Wu, X. Lu and Y. Tong, *Adv. Mater.*, 2017, **29**, 1700274.
17. S. Islam, M. H. Alfaruqi, V. Mathew, J. Song, S. Kim, S. Kim, J. Jo, J. P. Baboo, D. T. Pham, D. Y. Putro, Y.-K. Sun and J. Kim, *J. Mater. Chem. A*, 2017, **5**, 23299-23309.